Ionics (2021) 27:759–770
https://doi.org/10.1007/s11581-020-03866-1

ORIGINAL PAPER

Synthesis of transition metal oxide incorporated MOF-5 and NH_2-MOF-5 as efficient photoanode for oxygen evolution reaction

Muhammad Fiaz[1] · Dilshad Hussain[1,2] · Muhammad Athar[1]

Received: 17 September 2020 / Revised: 9 November 2020 / Accepted: 29 November 2020 / Published online: 2 January 2021

Abstract

Development of a highly active, stable, and facile-synthesized photoelectrocatalyst for water oxidation (OER) is very challenging and has attracted great research attention. In this article, highly efficient MOF-based photoelectrocatalysts (MOF-5 and amine-functionalized MOF (NH_2-MOF-5)) have been synthesized at room temperature and have been successfully characterized. For the photoelectrochemical studies, working electrodes are prepared by coating the synthesized photoelectrocatalysts on Ni-foam. All the synthesized materials have been successfully characterized via powder X-ray diffraction (PXRD), Fourier-transform infrared (FTIR) spectroscopy, scanning electron microscopy (SEM), energy-dispersive X-ray (EDX) spectroscopy, elemental mapping, and ultraviolet-visible (UV-Vis) spectroscopy. Photoelectrochemical measurements for oxygen evolution reaction are performed via cyclic voltammetry and linear sweep voltammetry. It has been observed that among all the synthesized catalysts, Co_3O_4@NH_2-MOF-5/NF has emerged as an efficient, stable, and highly active photoelectrocatalyst towards oxygen evolution reaction (OER) as compared to all other synthesized catalysts. It requires just 223 mV overpotential to deliver the 10 mA cm^{-2} current density and exhibits the lowest Tafel slope 52 mV dec^{-1} as compared to all other synthesized samples and some of the previously reported catalysts. Furthermore, long-term catalytic stability is studied via continuous linear sweep voltammetry and chronoamperometric measurements. This study encourages the development of a more efficient MOF-based catalyst for different photoelectrochemical studies.

Keywords Water oxidation · Oxygen evolution reaction · Amine-functionalized MOFs · Co_3O_4 · Linear sweep voltammetry

Introduction

In the twenty-first century, society is facing a great challenge to deal with environmental pollution and energy crisis due to dependence on carbon-based fuels. So, it motivated a huge number of scientists and researchers to search for an alternate source of energy [1]. Different strategies have been proposed to solve this and one of them is hydrogen production from water splitting. Water splitting is divided into two half-reactions: cathodic half-reaction (where hydrogen evolution reaction (HER) takes place) and anodic half-reaction (where oxygen evolution reaction (OER) takes place) [2]. Both HER and OER are kinetically sluggish reactions and huge overpotential is required to occur at a suitable rate. OER is four electron-proton coupled reaction ($4OH^- \rightarrow 2H_2O + 4e^- + O_2$) while HER is just a two-electron transfer reaction ($2H^+ + 2e^- \rightarrow H_2$). So, OER is kinetically more sluggish and requires higher overpotential as compared to HER to overcome the energy barrier and splits the water [3].

Therefore, extensive research has been focused on the development of highly efficient OER catalysts. Among various active OER catalysts, RuO_2 and IrO_2 are considered as highly active OER catalysts both in acidic and basic electrolytes because they require very less overpotential for oxygen evolution from water splitting [4, 5]. But, they cannot be used in large-scale practical applications due to their scarcity and expensive nature. So, researchers and scientists have devoted their research attention to the development of efficient, stable, and cost-effective non-noble metal OER catalysts, i.e., 3d-transition metal oxides, perovskites, transition metal sulfides, hydroxides, and non-metal compounds [6–10].

✉ Muhammad Athar
athar.qr@bzu.edu.pk

[1] Institute of Chemical Sciences, Bahauddin Zakariya University, Multan 60800, Pakistan

[2] HEJ Research Institute of Chemistry, International Centre for Chemical and Biological Sciences, University of Karachi, Karachi 75270, Pakistan

Metal-organic frameworks (MOFs) are porous crystalline-materials, composed of inorganic metal and an organic ligand. Due to their unique properties such as high porosity and large surface area, they have been widely used in a large number of potential applications such as gas adsorption/separation [11], magnetism [12], optoelectronics [13], and catalysis [14]. In recent years, due to their tunable pore structure and easy functionalization, MOFs are emerging as promising catalysts in a basic medium for water splitting [15]. Recently, highly efficient MOF-based OER catalysts have been reported such as NiFe-MOF-74 supported on Ni-foam delivered the benchmark of 10 mA cm^{-2} at 223 mV overpotential [16]. Similarly, Fe-doped Ni-MOF $Fe^{II}_{0.1}Ni_{0.4}$-MOF, Co-BPDC/Co-BDC heterojunction, UTSA-16, and Co-MOF have been reported as efficient OER catalysts and they delivered the 10 mA cm^{-2} current density at 294, 335, 408, and 360 mV overpotential, respectively [17–20]. Therefore, metal-organic frameworks (MOFs) have been used as potential catalysts for oxygen evolution reaction (OER), oxygen reduction reaction (ORR), and hydrogen evolution reaction (HER) such as NiO-MOF/rGo, rGO-NiO/CuO MOF, Ni-BTC-MOF/rGO, Co-BTC MOF/rGO, MnBDC@rGO, Cu-ZIF-67, NiCo/graphene, NiCo-ZIF, Cu-MOF/GO, and NiCo/NCNTs [21–30]. It has been also observed that catalytic efficiency of MOFs can be further increased by using 2-aminoterephthalic acid as an organic linker instead of terephthalic acid because amine functionalization shifts the band gap towards the visible region, increases the absorption of visible light, improves the charge separation, and reduces the e^-/h^+ (electron-hole pair) recombination [31].

First row 3d-transition metal oxide nanoparticles have been widely used in catalytic applications due to their low band gap, non-irritating, easy availability, and cost-effectiveness. Transition metal oxide (Mn, Fe, Co, Ni, and Cu) is also used as efficient HER and OER catalysts [32].

Therefore, in this research, we report the facile and low-cost synthesis of highly efficient OER M_xO_y@MOF-5 and M_xO_y@NH_2-MOF-5 (M_xO_y = Co_3O_4, NiO, CuO, and ZnO) catalysts at room temperature via in situ incorporation of four metal oxide nanoparticles into host MOFs. It is observed that amine functionalization has increased the photoelectrocatalytic activity towards OER. M_xO_y@NH_2-MOF-5 photoelectrocatalysts show better OER activity as compared to M_xO_y@MOF-5 and some of previously reported MOF-based OER catalysts.

Experimental

Chemicals

Zinc acetate dihydrate ($Zn(CH_3COO)_2{\cdot}2H_2O$, Merck, 99.99%), 1,4-benzenedicarboxylic acid (H_2BDC, Merck, 99%), 2-aminoterephthalic acid (Merck, 99%), N,N-dimethylformamide (DMF, Merck, 99.8%), sodium hydroxide (NaOH, Merck, 97%), ethanol (CH_3CH_2OH, Merck, 95%), oleic acid ($C_{18}H_{34}O_2$, Merck, 99%), iron sulfate heptahydrate ($Fe_2(SO_4)_3{\cdot}7H_2O$, Merck, 21-23% Fe basis), cobalt acetate tetrahydrate ($Co(C_2H_3O_2)_2{\cdot}4H_2O$, Merck, 97%), ammonia solution (NH_4OH, Merck, 28%), nickel chloride hexahydrate ($NiCl_2{\cdot}6H_2O$, Merck, 97%), copper nitrate trihydrate ($Cu(NO_3)_2{\cdot}3H_2O$, Merck, 99%), and deionized water.

Synthesis of transition metal oxide (M_xO_y) nanoparticles

Four transition metal oxide (M_xO_y = Co_3O_4, NiO, CuO and ZnO) nanoparticles were synthesized [33–36]. Except for Co_3O_4 nanoparticles, the remaining metal oxide (NiO, CuO, and ZnO) nanoparticles were synthesized by using the precipitation method. In brief, a particular amount of metal salt was dissolved in 100 mL distilled water by continuous stirring for 30 min. After that, 0.2 M NaOH was added dropwise and stirred for a specific period of time at a specific temperature as mentioned in Table 1. Then, precipitates were obtained, separated by centrifugation, washed with distilled water, and dried at 50 °C. After that, dried precipitates were calcinated at 500 °C for 2 h, while Co_3O_4 nanoparticles were prepared by using the one-step hydrothermal method. Cobalt acetate tetrahydrate was dissolved in distilled water by continuous stirring for 30 min. After that, 10 mL of ammonia solution was added dropwise under continuous stirring and transferred the whole mixture into Teflon-lined autoclave and heated at 180 ° C for 12 h. Finally, the precipitates of Co_3O_4 nanoparticles were obtained.

Synthesis of amine-functionalized MOF-5

MOF-5 was synthesized at room temperature. In a round-bottom flask, 2.7 g of $Zn(CH_3COO)_2{\cdot}2H_2O$ was dissolved into 100 mL DMF by continuous stirring. Then, 50 mL DMF solution containing 0.8 g H_2BDC was added dropwise to the mixture under constant magnetic stirring. The whole mixture was stirred at room temperature for 24 h. Precipitates were obtained, collected by centrifugation, and washed with distilled water and DMF several times. The resulting product was dried at 50 °C in a vacuum oven for 3 h.

Amine-functionalized MOF-5, NH_2-MOF-5, was synthesized under the same conditions as mentioned above for MOF-5 by using 2-aminoterephtahlic acid instead of 1,4-benzenedicarboxylic acid as an organic linker.

Table 1 Conditions for the synthesis of NiO, CuO, and ZnO nanoparticles via the precipitation method

Metal salt	Precipitating agent	Stirring time (h)	Temperature (°C)
Nickel chloride hexahydrate	Sodium hydroxide	2	50
Copper chloride	Sodium hydroxide	3	70
Zinc acetate dihydrate	Sodium hydroxide	2	60

Synthesis of M_xO_y@MOF-5 and M_xO_y@NH_2-MOF-5 composites

M_xO_y@MOF-5 and M_xO_y@NH_2-MOF-5 composites were synthesized at room temperature via in situ incorporation of pre-synthesized metal oxide nanoparticles into host MOFs. In a typical procedure, 0.8 g of 1,4-benzenedicarboxylic acid was dissolved in 20 mL DMF by continuous stirring for 30 min. After that, dropwise added 10 mL DMF suspension of 0.01 g metal oxide nanoparticles and 2.7 g/20 mL DMF solution of $Zn(CH_3COO)_2{\cdot}2H_2O$, respectively. Then, the resultant solution was continuously stirred for 24 h and precipitates were separated by centrifugation, washed with distilled water and DMF, and dried overnight at 50 °C in an oven under vacuum. In the same way, M_xO_y@NH_2-MOF-5 composites were synthesized by using 0.8 g/20 mL DMF of 2-aminoterephthalic acid instead of 1,4-benzenedicarboxylic acid.

Instruments

Powder X-ray diffraction spectra (PXRD) were obtained in 2θ range 5 to 80° via Shimadzu X-ray diffractometer with Cu-Kα radiation (λ = 0.15406 nm) at 40 kV and 40 mA. A Nicolet Nexus 870 spectrometer was used to collect FTIR spectra in the wavelength range from 400 to 4000 cm^{-1}. Morphology and elemental composition of synthesized samples were evaluated by using Philips XL30 Environmental SEM attached with an Oxford Instrument Inca 500 energy-dispersive X-ray spectrometer (EDX). Optical properties were studied by using Shimadzu UV-2600 spectrophotometer in the range of 200–900 nm.

Formation of working electrodes

The slurry of the catalyst was uniformly pasted on a piece (1 cm^2) of Ni-foam (NF) to form working electrodes. Before pasting slurry, Ni-foam was cleaned with acetone and water via sonication and dried at 50 °C in an oven for 2 h. To prepare the slurry, 10 mg of synthesized sample was dispersed in 1 mL deionized water via sonication for 30 min. After that, it was uniformly pasted on Ni-foam to form a photoanode for OER.

Photoelectrochemical studies

Photoelectrochemical studies towards OER were studied in a common three-electrode setup with Ag/AgCl as a reference electrode, Pt as a counter electrode, and catalyst coated on Ni-foam as photoanode. The photoelectrochemical studies were studied both in dark and in presence of visible light. The electrodes were dipped in 1M KOH $_{(aq)}$ electrolyte solution. A Uniscan instrument 3100 Poteniostat/Galvanostat attached with NOVA 1.10 software for automated data taking and recording was used for OER analysis. OER activity was studied via cyclic voltammetry (CV) and linear sweep voltammetry (LSV) measurements at 30 and 1 mV s^{-1}, respectively. All the potential data was converted into reversible hydrogen electrode (RHE) potential by using the following equation.

$$E_{RHE} = E_{Ag/AgCl/Sat.KCl} + 0.059\,pH + 0.197 \quad (1)$$

For OER, overpotential (η) was calculated by using the following equations

$$\eta = E_{RHE} - 1.23 \quad (2)$$

Tafel slope was calculated from the Tafel plot by using the following equation

$$\eta = a + b\log j \quad (3)$$

where η is the overpotential, j is the current density, and b is the Tafel slope

Furthermore, the stability of working electrodes was found via continuous 1000 LSV sweeps and chronoamperometric studies at an applied potential of 1.5 V in the presence of visible light.

Results and discussion

Crystallographic analysis

The powder X-ray diffraction patterns (PXRD) of bare MOF-5 and M_xO_y@MOF-5 in comparison with the simulated pattern of MOF-5 generated from original CIF file are represented in Fig. 1a. It can be seen that all the characteristic diffraction peaks of MOF-5 are consistent with the simulated pattern and it reveals the successful synthesis of

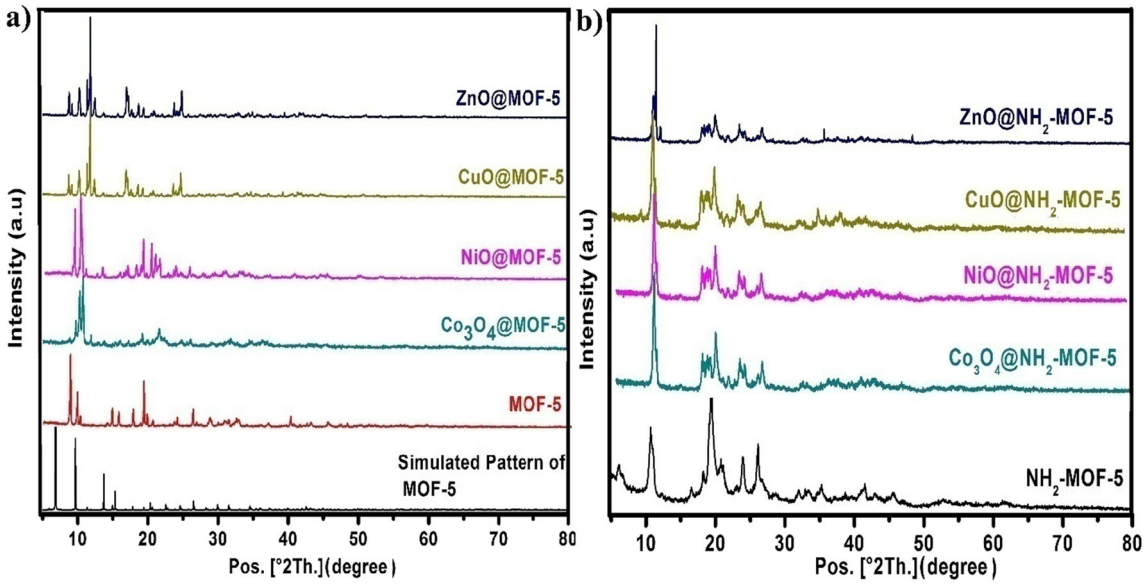

Fig. 1 **a** PXRD patterns of pure MOF-5, Co_3O@MOF-5, NiO@MOF-5, CuO@MOF-5, and ZnO@MOF-5 compared with the simulated pattern of MOF-5; **b** PXRD patterns of pure NH_2-MOF-5, Co_3O_4@NH_2-MOF-5, NiO@NH_2-MOF-5, CuO@NH_2-MOF-5, and ZnO@NH_2-MOF-5

Zn-based metal-organic framework, MOF-5. After the incorporation of metal oxide nanoparticles into MOF-5, M_xO_y@MOF-5 spectra exhibit some new diffraction peaks besides the diffraction peaks of MOF-5, which are in good agreement with the diffraction pattern of metal oxide (Co_3O_4, NiO, CuO, and ZnO) nanoparticles. Figure 1b represents the crystallographic patterns of NH_2-MOF-5 and M_xO_y@NH_2-MOF-5 composites. It is observed that NH_2-MOF-5 has a different crystal structure and PXRD pattern as compared to MOF-5 due to the use of 2-aminoterephtalic acid instead of simple terephthalic acid. However, like M_xO_y@MOF-5, PXRD spectra of M_xO_y@NH_2-MOF-5 indicate that amine-functionalized MOF, NH_2-MOF-5, maintains its crystal structure and remains intact after incorporation of metal oxide nanoparticles. No extra diffraction peaks for impurity are observed, which indicates the single-phase formation of all these samples. From powder XRD analysis of M_xO_y@MOF-5 and M_xO_y@NH_2-MOF-5, it can be concluded that incorporation of metal oxide nanoparticles does not significantly affect the crystalline structure of host MOFs, and there is no chemical interaction between incorporated nanoparticles and a central metallic cluster of MOFs; they are intact with each other via physical interaction.

Fourier-transform infrared spectroscopic analysis

The surface functional groups and formation of pure Zn-based MOFs MOF-5 and NH_2-MOF-5 as well as their composites M_xO_y@MOF-5 and M_xO_y@NH_2-MOF-5 are confirmed by FTIR spectroscopy. Figure 2a represents the FTIR spectra of MOF-5 and M_xO_y@MOF-5 composites. In the FTIR spectrum of MOF-5, two strong transmittance peaks related to symmetric and asymmetric stretching vibrations of the carboxylic group are observed at 1575 and 1375 cm^{-1}. A weak transmittance peak can also be seen at 642 cm^{-1} due to symmetric stretching vibration of the central Zn_4O^{6+} cluster of MOF-5 [37]. However, in the FTIR spectrum of NH_2-MOF-5, a weak peak is observed at 1242 cm^{-1} for C–N stretching vibration of the aromatic amine group and two strong transmittance peaks are also observed at 1540 and 1378 cm^{-1} indexed to the vibrational motion of carboxylate group of 2-aminoterephthalic acid, shown by Fig. 2b [38], while FTIR spectra of M_xO_y@MOF-5 and M_xO_y@NH_2-MOF-5 composites exhibit some additional peaks at 576, 517, 535, and 555 cm^{-1} for vibrations of Co–O, Ni–O, Cu–O, and Zn–O [39–41], respectively in addition to vibrational bands of both Zn-based MOFs MOF-5 and NH_2-MOF-5, which indicates that metal oxide nanoparticles have been successfully incorporated into MOFs.

Morphological and compositional analysis

The morphology and composition of all the synthesized samples have been studied by scanning electron microscopy images, SEM-based energy-dispersive X-ray (EDX) analysis, and elemental mapping. Figure 3A (a–e) represents the SEM images of synthesized bare MOF-5 and M_xO_y@MOF-5 composites. It appears that synthesized MOF-5 has grown in well-defined rectangular morphology and is uniformly distributed, shown by Fig. 3A (a). Similarly, the incorporated samples, M_xO_y@MOF-5, have also grown in almost rectangular morphology but due to the incorporation of metal oxide nanoparticle coarse surfaces, variations in size and slight

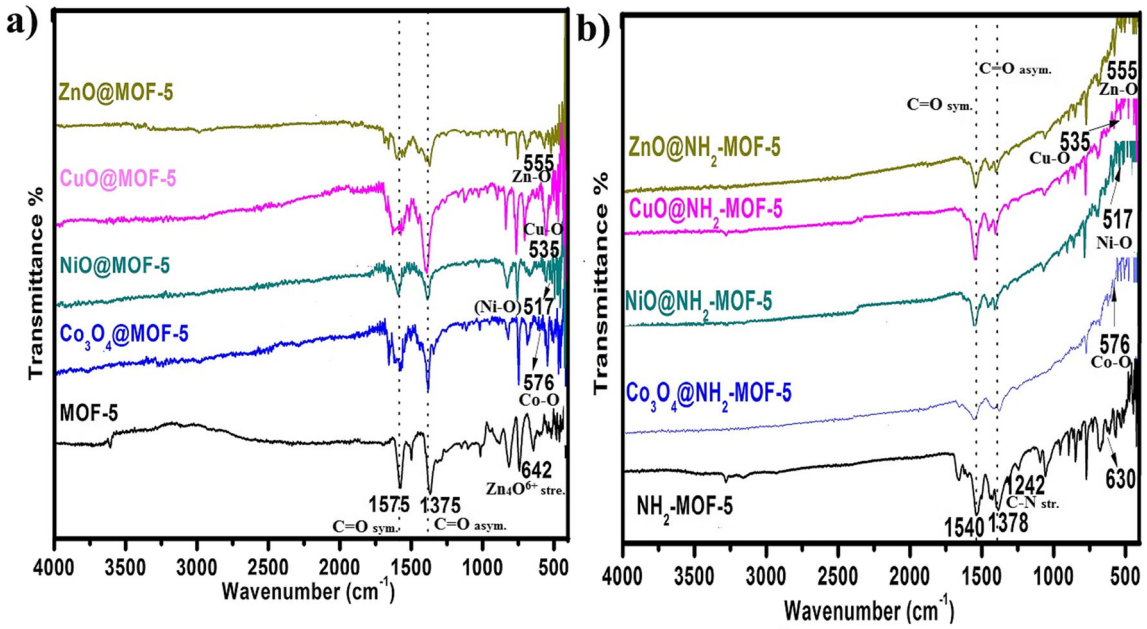

Fig. 2 **a** FTIR spectrum of pure MOF-5, Co_3O@MOF-5, NiO@MOF-5, CuO@MOF-5, and ZnO@MOF-5; **b** FTIR spectrum of NH_2-MOF-5, Co_3O_4@NH_2-MOF-5, NiO@NH_2-MOF-5, CuO@NH_2-MOF-5, and ZnO@NH_2-MOF-5

agglomerations are also observed, represented by Fig. 3A (b-e). Figure 3A (a′–e′) represents the SEM-based mix elemental maps of synthesized MOF-5 and its composites. It indicates that metal oxide nanoparticles have been successfully incorporated into cavities of MOF-5 and these particles are uniformly distributed.

The SEM images reveal that bare amine-functionalized MOF NH_2-MOF-5 and its composites M_xO_y@NH_2-MOF-5 have grown in spherical shapes with spongy smooth surfaces, as shown in Fig. 3B (a–e). However, as a result of the incorporation of metal oxide nanoparticles, some variations in size and agglomeration are observed in incorporated samples. Mix elemental maps of M_xO_y@MOF-5 and M_xO_y@NH_2-MOF-5 indicate that metal oxide nanoparticles have been successfully incorporated into cavities of both Zn-based MOFs and these particles are uniformly distributed, as shown in Fig. 3B (a′–e′). Individual elemental maps of basic components of bare MOFs (MOF-5 and

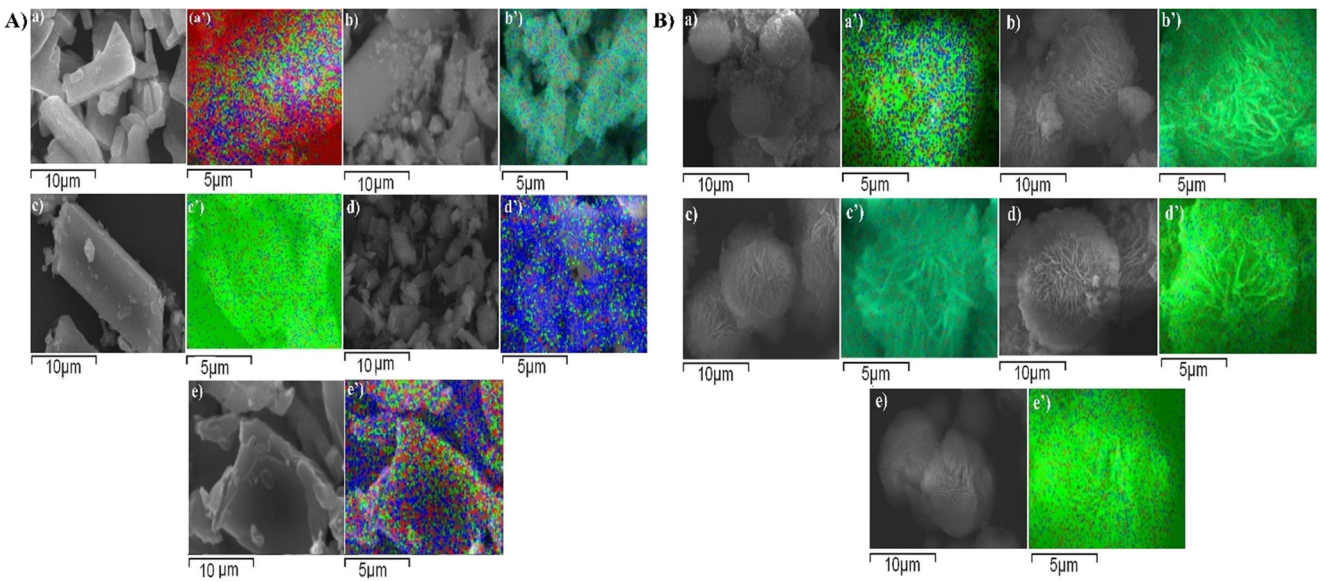

Fig. 3 A) SEM (a–e) and SEM-based mix elemental maps (a′–e′) of MOF-5, Co_3O@MOF-5, NiO@MOF-5, CuO@MOF-5, and ZnO@MOF-5, respectively; B) SEM (a–e) and SEM-based mix elemental maps (a′–e′) of NH_2-MOF-5, Co_3O_4@NH_2-MOF-5, NiO@NH_2-MOF-5, CuO@NH_2-MOF-5, and ZnO@NH_2-MOF-5, respectively

NH_2-MOF-5) and their composites (M_xO_y@MOF-5 and M_xO_y@NH_2-MOF-5) are shown in Figure S1 and S2.

The composition of all the synthesized samples has been studied through SEM-based EDX images. Figure S3 and S4 represent the EDX images of MOF-5/M_xO_y@MOF-5 and NH_2-MOF-5/M_xO_y@NH_2-MOF-5, respectively. It is evaluated from EDX images of bare MOF-5 and NH_2-MOF-5 that they only contain diffraction peaks of basic elements Zn, C, and O of MOF-5 and Zn, C, O, and N of NH_2-MOF-5, respectively. Similarly, incorporated samples contain all basic diffraction peaks of their respective MOF and they also contain additional diffraction peaks of Co, Cu, Ni, and Zn. It indicates the successful incorporation of metal oxide nanoparticles into both Zn-based MOFs. No additional peak of impurity is observed, which indicates a high degree of purity of these synthesized samples.

Optical analysis

The UV-Vis absorption spectra of as-synthesized bare Zn-based MOF MOF-5 and amine-functionalized MOF NH_2-MOF-5 as well as their composites are represented by Fig. 4a, b. Figure 4a shows that MOF-5 exhibits maximum absorption at 207 nm with an absorption edge at 320 nm due to the organic linker terephthalate and inorganic central Zn_4O_{13} cluster. It indicates that in MOF-5 ligand-to-metal charge transfer (LMCT) takes place. Upon loading with metal oxide nanoparticles into MOF-5, a redshift is observed in the UV region with maximum absorption at 235, 213, 245, and 256 nm in Co_3O_4@MOF-5, NiO@MOF-5, CuO@MOF-5, and ZnO@MOF-5, respectively. It has been also observed that in M_xO_y@MOF-5, absorption edges have extended up to 400 nm and new absorption peaks are also

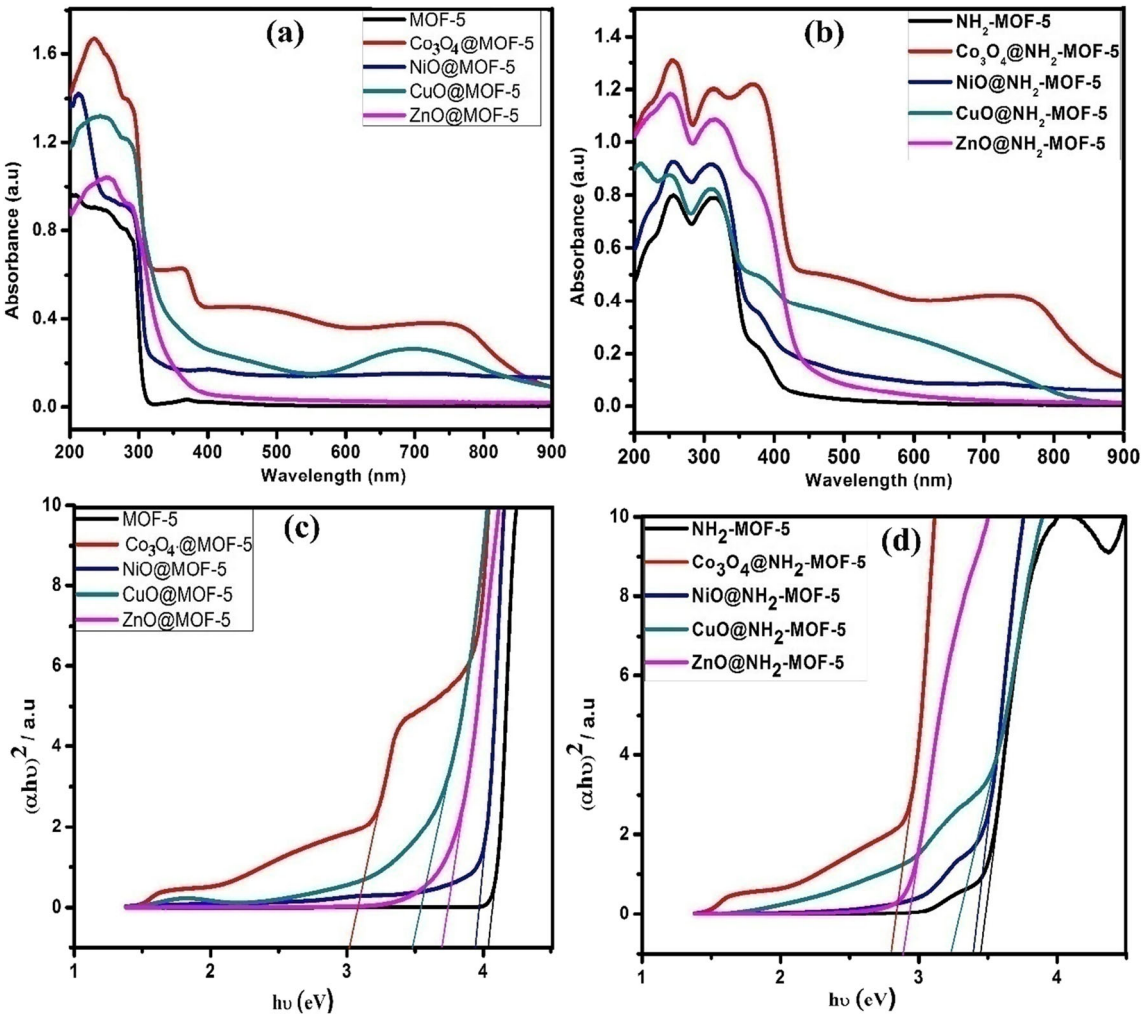

Fig. 4 **a** UV-Vis absorption spectra of MOF-5, Co_3O@MOF-5, NiO@MOF-5, CuO@MOF-5, and ZnO@MOF-5; **b** UV-Vis absorption spectra of NH_2-MOF-5, Co_3O_4@NH_2-MOF-5, NiO@NH_2-MOF-5, CuO@NH_2-MOF-5, and ZnO@NH_2-MOF-5; **c** Tauc plot of MOF-5, Co_3O@MOF-5, NiO@MOF-5, CuO@MOF-5, and ZnO@MOF-5; **d** Tauc plot of NH_2-MOF-5, Co_3O_4@NH_2-MOF-5, NiO@NH_2-MOF-5, CuO@NH_2-MOF-5, and ZnO@NH_2-MOF-5

observed in the visible region with λ_{max} at 695 and 754 nm in Co_3O_4@MOF-5 and CuO@MOF-5, respectively. The band gap of all these synthesized samples has been calculated from the Tauc plot, Fig. 4c, and is 4.03,3.01, 3.94, 3.48, and 3.70 eV for MOF-5, Co_3O_4@MOF-5, NiO@MOF-5, CuO@MOF-5, and ZnO@MOF-5, respectively. All these MOF-5-based samples exhibit low efficiency towards water splitting due to a large effective band gap. Therefore, their efficiency has been further improved by the amine-functionalization of MOF-5. The water-splitting efficiency of NH_2-MOF-5 is significantly improved due to amine functionality. NH_2-MOF-5 exhibits absorption edge at around 438 nm and upon loading with metal oxide nanoparticles, M_xO_y@NH_2-MOF-5 composites, absorption edges extend up to 600 nm, falling in the visible region, as shown in Fig. 4b. So, a significant redshift is observed. Their calculated band gaps are 3.45, 2.78, 3.39, 3.23, and 2.89 eV for NH_2-MOF-5, Co_3O_4@NH_2-MOF-5, NiO@NH_2-MOF-5, CuO@NH_2-MOF-5, and ZnO@NH_2-MOF-5, respectively. It indicates that amine functionalization reduces the band gap, increases the charge separation, and improves the catalytic activity.

Photoelectrochemical studies towards oxygen evolution reaction

Photoelectrochemical studies towards oxygen evolution reaction are studied by cyclic voltammetry (CV) and linear sweep voltammetry (LSV) at 30 and 1 mV s^{-1}, respectively. Photoelectrochemical studies towards OER are studied both in dark and in the presence of visible light. Figure 5a represents the CV curves of MOF-5/NF and M_xO_y@MOF-5/NF electrodes. It is observed that almost zero current density is produced in dark due to negligible OER activity. However, all the synthesized samples exhibit anodic current density under illumination which further increases gradually with the incorporation of pre-synthesized nanoparticles. The bare MOF-5/NF generates only 0.012 mA cm^{-2} current density and after incorporation of metal oxide nanoparticles, a tremendous increase in current density has been observed in M_xO_y@MOF-5/NF electrodes and among all these catalysts, Co_3O_4@MOF-5/NF shows the lowest onset potential and generates maximum current density for OER. The catalytic OER activity of these synthesized samples has been further increased by amine functionalization of terephthalic acid. Figure 5b represents the CV curves of synthesized NH_2-MOF-5/NF and M_xO_y@NH_2-MOF-5/NF. It can be observed from CV curves that after amine functionalization, lower onset potential and higher current density are achieved towards OER as compared to bare MOF-5/NF and M_xO_y@ MOF-5/NF, respectively. Like M_xO_y@MOF-5/NF, among M_xO_y@NH_2-MOF-5/NF electrodes, Co_3O_4@NH_2-MOF-5/NF shows the lowest onset potential and generates the highest 34.48 mA cm^{-2} current density as compared to bare NH_2-MOF-5/NF (6.33 mA cm^{-2}), NiO@NH_2-MOF-5/NF (8.06 mA cm^{-2}), CuO@NH_2-MOF-5/NF (16.77 mA cm^{-2}), and ZnO@NH_2-MOF-5/NF (20.67 mA cm^{-2}), respectively.

Figure 5c and d represent the LSV curves of bare MOF-5 and amine-functionalized MOF, NH_2-MOF-5/NF-based electrodes, and it can be seen that amine-functionalized-based electrodes exhibit better OER activity as compared to non-amine-functionalized working electrodes. It is also observed that the Co_3O_4@NH_2-MOF-5/NF electrode exhibits the largest current density (32.93 mA cm^{-2} at 1.49 V vs. RHE) for OER as compared to all other electrodes. For comparison, overpotential (η) requires to achieve 5 mA cm^{-2} current density is considered, represented by Fig. 5e, f. It is found that Co_3O_4@NH_2-MOF-5/NF needs only 203 mV overpotential to deliver 5 mA cm^{-2} as compared to all other amine-functionalized-based electrodes NH_2-MOF-5/NF (η_5 = 353 mV), NiO@NH_2-MOF-5/NF (η_5 = 243 mV), CuO@NH_2-MOF-5/NF (η_5 = 223 mV), and ZnO@NH_2-MOF-5/NF (η_5 = 333 mV) as well as non-amine-functionalized-based electrodes Co_3O_4@MOF-5/NF (η_5 = 323 mV), NiO@MOF-5/NF (η_5 = 353 mV), CuO@MOF-5/NF (η_5 = 343 mV), and ZnO@MOF-5/NF (η_5 = 333 mV). Furthermore, the overpotential required to reach the benchmark of 10 mA cm^{-2} current density is compared and it has been found that Co_3O_4@NH_2-MOF-5/NF requires the lowest 223 mV overpotential to deliver 10 mA cm^{-2} as compared to both amine-functionalized and non-amine-functionalized-based electrodes CuO@NH_2-MOF-5/NF (η_{10} = 253 mV), ZnO@NH_2-MOF-5/NF (η_{10} = 353 mV), Co_3O_4@MOF-5/NF (η_{10} = 343 mV), NiO@MOF-5/NF (η_{10} = 363 mV), and CuO@MOF-5/NF (η_{10} = 353 mV), represented by Fig. 6a. This indicates that the Co_3O_4@NH_2-MOF-5/NF electrode is a highly efficient photoelectrocatalyst for photoelectrochemical OER as compared to all other synthesized photoelectrocatalysts as well as previously reported Co-based and MOF-based OER catalysts, as represented in Table 2.

Tafel slope is an important parameter to understand the reaction kinetics. So, the Tafel plot is derived from LSV curves of MOF-5/NF and NH_2-MOF-5/NF-based electrodes, as shown by Fig. 6b, c. It is revealed from Tafel plots that amine-functionalized electrodes show a lower Tafel slope as compared to non-amine-functionalized-based electrodes, which indicates that amine-functionalized electrodes have more favorable electron transfer and better OER activity. It is observed that Co_3O_4@NH_2-MOF-5/NF exhibits the lowest Tafel slope 52 mV dec^{-1} as compared to all other synthesized catalysts as well as previously reported MOF-based OER catalysts as shown in Table 2. This result agrees with the highest current density of Co_3O_4@NH_2-MOF-5/NF towards OER activity. So, it can be concluded that Co_3O_4@NH_2-MOF-5/NF is a highly efficient catalyst for OER as compared to all

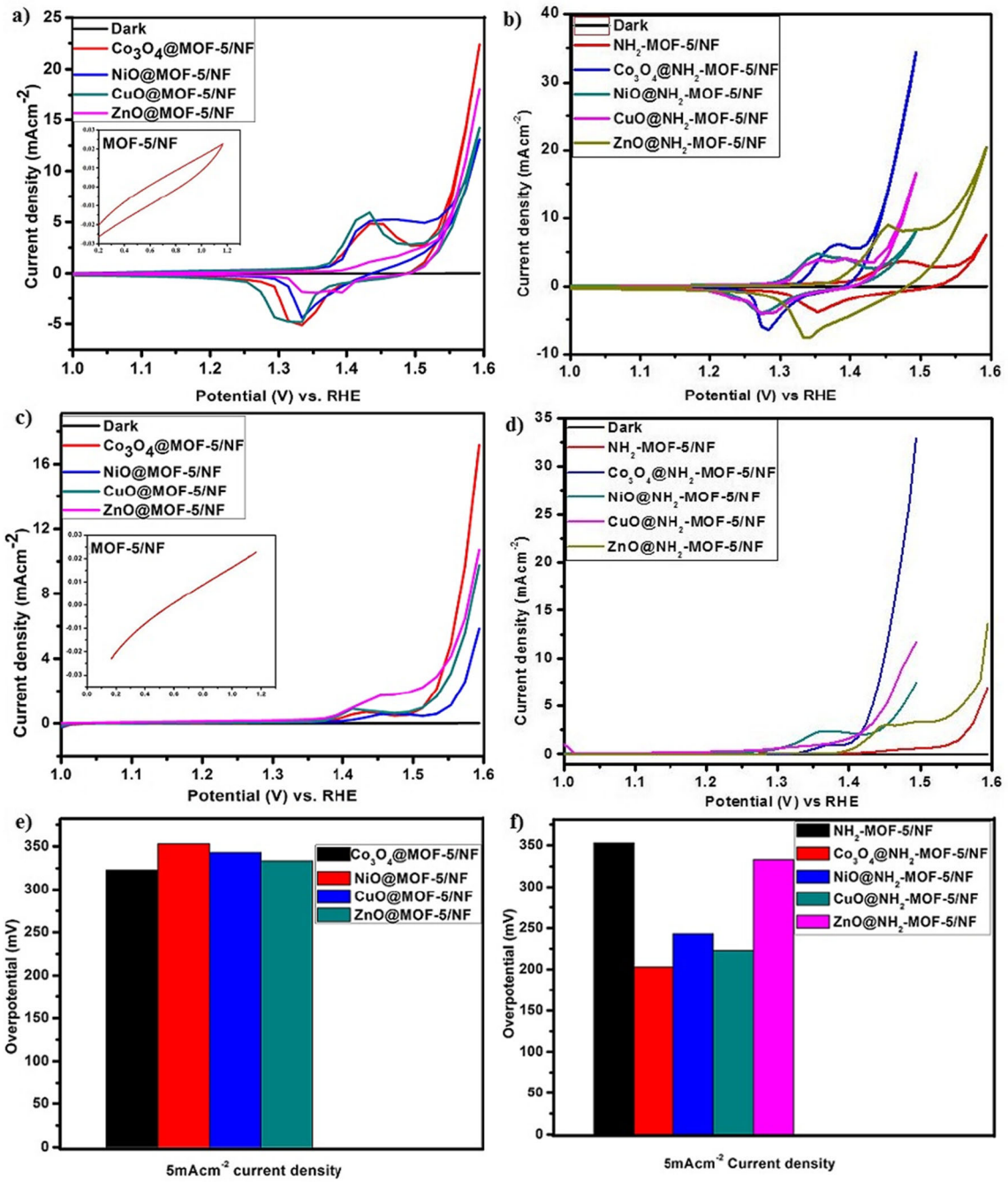

Fig. 5 **a** and **b** CV curves of bare MOF-5/NF, NH_2-MOF-5/NF, and their composites, respectively; **c** and **d** LSV curves of bare MOF-5/NF, NH_2-MOF-5/NF, and their composites, respectively; **e** and **f** overpotential required to 5 mA cm^{-2} current density for MOF-5- and NH_2-MOF-5-based composites

synthesized photoelectrocatalysts. It is expected that in basic medium, OER is occurred by the following equations

$$OH^- \rightarrow OH_{ads} + e^- \quad (4)$$

$$OH_{ads} + OH^- \rightarrow O_{ads} + H_2O + e^- \quad (5)$$

$$O_{ads} + OH^- \rightarrow OOH_{ads} + e^- \quad (6)$$

$$OOH_{ads} + OH^- \rightarrow O_{2(g)} + e^- \quad (7)$$

So, this overall catalytic OER study reveals that amine functionalization of MOF-5 by using 2-aminoterephthalic acid has shifted the band gap towards the visible region, increased the charge separation, enhanced the absorption of visible light, and improved the photoelectrocatalytic OER activity. Thus, amine functionalization of MOF-5 has significantly enhanced the OER activity via water splitting.

Table 2 Comparison of the OER activity of Co_3O_4@NH_2-MOF-5/NF with previously reported Co- and MOF-based materials in literature

Electrocatalyst	Electrolyte	Overpotential (mV) for 10 mA cm^{-2} current density	Tafel slope (mV dec^{-1})	Reference
$Fe^{II}_{0.1}Ni_{0.4}$-MOF	1.0 M KOH	294	47.45	Chem. Pap. (2020)
$NiCo_2O_4$-3D nanoflower	1.0 M KOH	383	137	Int. J. Hydrogen energy (2019) 44, 16120-16131
Co_3O_4/rGO-W	1.0 M KOH	382	62	Electrochim. Acta (2019) 300, 123-130
CoS_2-$NiCo_2S_4$/NSG	1.0 M KOH	272	62.8	Appl. Surf.Sci. (2020) 503, 144146
Co-BPDC/Co-BDC heterojunction	1.0 M KOH	335	72.1	Inorg. Chem. (2020) 59, 1295-1305
UTSA-16	1.0 M KOH	408	77	ACS Appl. Mater. Interfaces (2017) 9, 7193−7201
Co-MOF	1.0 M KOH	360	89	Polymers (2017) 9, 676.
Co_3O_4@NH_2-MOF-5/NF	1.0 M KOH	*223*	*52*	This work

The stability of the working electrode is another important parameter for photoelectrochemical studies. Therefore, the stability of Co_3O_4@MOF-5/NF and Co_3O_4@NH_2-MOF-5/NF is studied by 1000 continuous LSV sweeps. Figure 7a and b represent the 1st and 1000th LSV cycle of Co_3O_4@MOF-5/NF and Co_3O_4@NH_2-MOF-5/NF, respectively. It reveals that there is no degradation in current density before and after the 1000th LSV cycle. In addition to 1000 LSV cycles, long-term photoelectrocatalytic stability is also important for commercial applications. The long-term stability of all the synthesized samples is carried out for 6000 s by using the chronoamperometry technique. Figure 7c and d show the current vs. time graph of all the synthesized working electrodes at the static potential of 1.5 V vs. RHE for MOF-5-based and NH_2-MOF-5-based working electrodes, respectively in the presence of visible light. The stability study reveals the satisfactory and superior stability of Co_3O_4@NH_2-MOF-5/NF photoelectrocatalyst towards OER in alkaline solution.

Another important parameter to study reaction kinetics is impedance spectroscopy (EIS). It gives an idea about solution induced resistance as well as resistance at electrode/electrolyte interface (charge transfer resistance). The small diameter of semicircle indicates low induced resistance, low charge transfer resistance, and higher catalytic activity. Figure S5 represents the Nyquist plot of Co_3O_4@NH_2-MOF-5/NF and bare MOF NH_2-MOF-5. It shows that Co_3O_4@NH_2-MOF-5/NF has a small diameter of the semicircle as compared to bare MOF NH_2-MOF-5/NF, which reveals that Co_3O_4@NH_2-MOF-5/NF has low charge transfer resistance, maximum conductance, and better OER activity as compared to bare MOF NH_2-MOF-5/NF.

Proposed mechanism of photoelectrochemical oxygen evolution reaction

In MOFs, organic linkers act as an antenna, capture the visible light, and generate the photogenerated electrons. Therefore, it is hypothesized that photogenerated electrons are transferred from the valence band of NH_2-MOF-5 to its conduction band and subsequently transferred to the energy level of incorporated Co_3O_4 nanoparticles. Furthermore, these electrons are transferred to the counter electrode via an external circuit and increased the charge separation, reduced the electron-

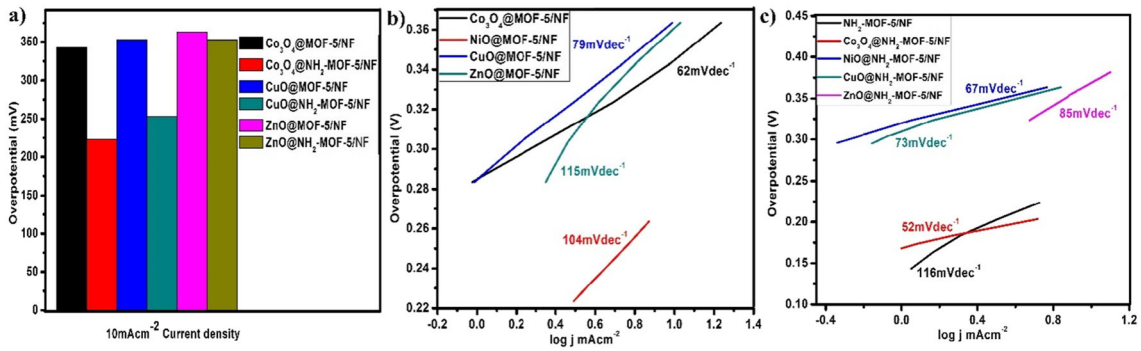

Fig. 6 **a** Overpotential required to achieve the 10 mA cm^{-2} current density; **b** Tafel plot of MOF-5-based composites; **c** Tafel plot of NH_2-MOF-5-based samples

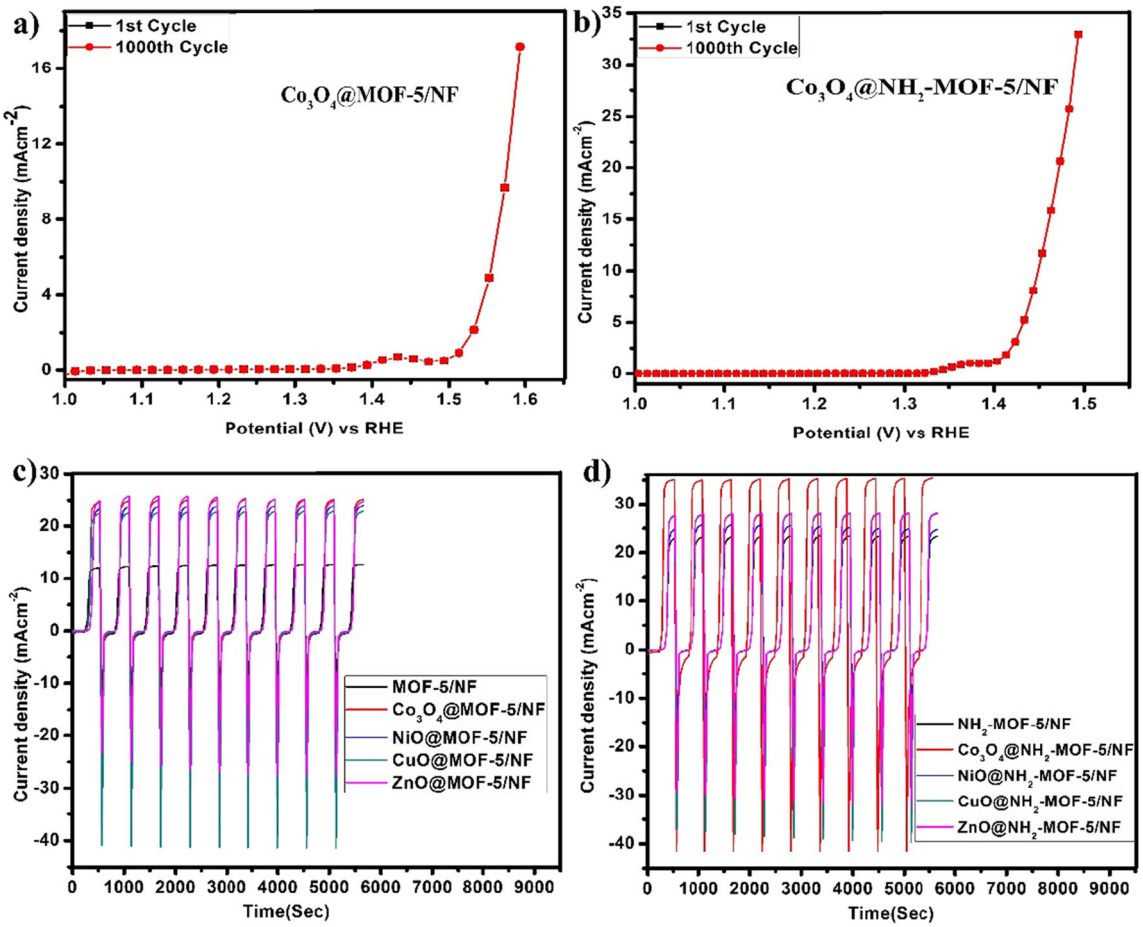

Fig. 7 **a** and **b** 1st and 1000th LSV cycle of Co_3O_4@MOF-5/NF and Co_3O_4@NH_2-MOF-5/NF, respectively; **c** and **d** long-term stability test of all MOF-5-based and NH_2-MOF-5-based photoelectrocatalysts

hole pair recombination, and enhanced the catalytic activity. The resulting holes at the surface of the photoanode cause the photooxidation of water into O_2 and H^+. The H^+ is transported towards the counter electrode via electrolyte where they undergo photoreduction by photogenerated electrons and generate hydrogen gas, as shown in Fig. 8.

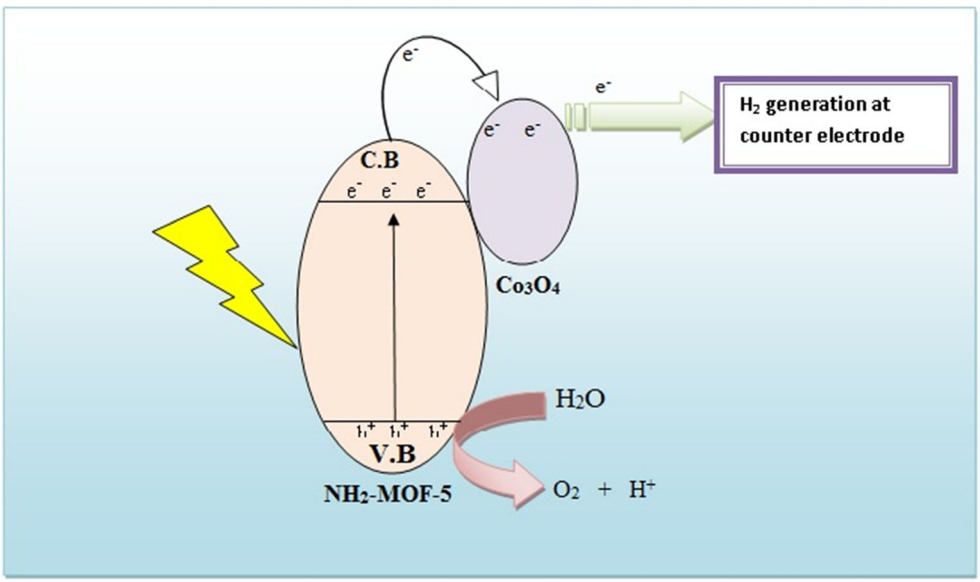

Fig. 8 Proposed mechanism for electron transfer and oxygen evolution reaction by Co_3O_4@NH_2-MOF-5 under sunlight exposure

Conclusion

In summary, the photoelectrocatalytic activity towards water oxidation (OER) of MOF-5-based photoelectrocatalysts has been successfully increased by amine functionalization. So, NH_2-MOF-5/NF and M_xO_y@NH_2-MOF-5/NF photoelectrocatalysts exhibit better and enhanced catalytic activity towards OER as compared to MOF-5/NF and M_xO_y@MOF-5/NF catalysts. Among all the synthesized photoelectrocatalysts, Co_3O_4@NH_2-MOF-5/NF exhibits excellent catalysis towards OER in alkaline medium and it requires the lowest overpotential 203 mV and 223 mV to delivers 5 and 10 mA cm^{-2}, respectively. In addition, it exhibits the lowest Tafel slope of 52 mV dec^{-1} and excellent long-term stability as compared to all other synthesized catalysts. A large number of active sites, fast electron transfers, and reduce electron-hole pair recombination lead to enhance the OER activity of Co_3O_4@NH_2-MOF-5/NF as compared to all other synthesized catalysts and even some of the previously reported catalysts. This study encourages the development of more nanoparticles incorporated amine-functionalized MOF-based photoelectrocatalysts and used them in electrocatalytic applications.

Supplementary Information The online version contains supplementary material available at https://doi.org/10.1007/s11581-020-03866-1.

Acknowledgments The authors acknowledge Prof. Duncan H. Gregory, School of Chemistry, University of Glasgow, UK, for providing the lab facilities.

Compliance with ethical standards

Conflict of interest The authors declare that they have no conflict of interest.**Supplementary Information** The online version contains supplementary material available at https://doi.org/10.1007/s11581-020-03866-1.

References

1. Panwar NL, Kaushik SC, Kothari S (2011) Role of renewable energy sources in environmental proection: a review. Renew Sust Energ Rev 15:1513–1524
2. Zhang L, Xiao J, Wang H, Shao M (2017) Carbon-based electrocatalysts for hydrogen and oxygen evolution reactions. ACS Catal 7:7855–7865
3. Zhao X, Pattengale B, Fan D, Zou Z, Du J, Huang J, Xu C (2018) Mixed-node metal-organic framework as efficient electrocatalysts for oxygen evolution reaction. ACS Energy Lett 3:2520–2526
4. Zhao LL, Cao Q, Wang AL, Duan JZ, Zhou WJ, Sang YH, Liu H (2018) Iron oxide embedded titania nanowires-an active and stable electrocatalyst for oxygen evolution in acidic media. Nano Energy 45:118–126
5. Wang L, Wu YZ, Cao R, Ren LT, Chen MX, Feng X, Zhou JW, Wang B (2016) Fe/Ni metal-organic frameworks and their binder-free thin films for efficient oxygen evolution with low overpotential. ACS Appl Mater Interfaces 8:16736–16743
6. Lu Z, Wang H, Kong D, Yan K, Hsu PC, Zheng G, Yao H, Liang Z, Sun X, Cui Y (2014) Electrochemical tuning of layered lithium transition metal oxides for improvement of oxygen evolution reaction. Nat Commun 5:4345
7. Sun Y, Gao S, Lei F, Liu J, Liang L, Xie Y (2014) Atomically-thin non-layered cobalt oxide porous sheets for highly efficient oxygen-evolving electrocatalysts. Chem Sci 5:3976–3982
8. Gao M, Sheng W, Zhuang Z, Fang Q, Gu S, Jiang J, Yan Y (2014) Efficient water oxidation using nanostructured α-nickel-hydroxide as an electrocatalyst. J Am Chem Soc 136:7077–7084
9. Jung JI, Jeong HY, Lee JS, Kim MG, Cho J (2014) A bifunctional perovskite catalyst for oxygen reduction and evolution. Angew Chem Int Ed 53:4582–4586
10. Delgado D, Minakshi M, Senanayake G, Kim D (2015) Modified electrolytic manganese dioxide (MEMD) for oxygen generation in alkaline medium. J Solid State Electrochem 19:1133–1142
11. Rosi NL, Eckert J, Eddaoudi M (2003) Hydrogen storage in microporous metal-organic frameworks. Science 300:1127–1129
12. Zhang WX, Yang YY, Zai SB (2008) Syntheses, structures and magnetic properties of dinuclear copper (II)-lanthanide (III) complexes bridged by 2-hydroxymethyl-1-methylimidazole. Eur J Inorg Chem 2008:679–685
13. Moore EG, Samuel APS, Raymond KN (2009) From antenna to assay: lessons learned in lanthanide luminescence. Acc Chem Res 42:542–552
14. Jahan M, Liu Z, Loh KP (2013) A Graphene oxide and copper-centered metal organicframework composite as a tri-functional catalyst for HER, OER, and ORR. Adv Funct Mater 23:5363–5372
15. Xiaohua Z, Brian P, Donghua F, Zehua Z, Yongqing Z, Jing D, Jier H, Cailing X (2018) Mixed-node metal-organic frameworks as efficient electrocatalysts for oxygen evolution reaction. ACS Energy Lett 3:2520–2526
16. Xing J, Guo K, Zou Z, Cai M, Du J, Xu C (2018) In situ growth of well-ordered NiFe-MOF-74 on Ni foam by Fe^{2+} induction as an efficient and stable electrocatalyst for water oxidation. Chem Commun 54:7046–7049
17. Dandan Z, Renxing H, Huaming X, Ruizhen L, Xingyong L, Ming P, Ying L (2020) Effect of the valence state of initial iron source on oxygen evolution activity of Fe-doped Ni-MOF. Chemical Paper
18. Qingqing Z, Feifei Y, Guoxu Q, Yonghong N (2020) Cobalt-based MOF-on-MOF two-diemensional heterojunction nanostructures for enhanced oxygen evolution reaction electrocatalytic activity. Inorg Chem 59:1295–1305
19. Jiang J, Huang L, Liu MX, Ai HL (2017) Bioinspired cobalt-citrate metal-organic framework as an efficient electrocatalyst for water oxidation. ACS Appl Mater Interfaces 9:7193–7201
20. Meng GQ, Yang JJ, Ma XS, Zhai JM, Lu TJ (2017) A porous cobalt (II) metal-organic framework with highly efficient electrocatalytic activity oxygen evolution reaction. Polymers 9:676
21. Noor T, Zaman N, Nasir H, Iqbal N, Hussain Z (2019) Electro catalytic study of NiO-MOF/rGO composite for methanol oxidation reduction. Electrochim Acta 307:1–12
22. Noor T, Pervaiz S, Iqbal N, Nasir H, Zaman N, Sharif M, Pervaiz E (2020) Nanocomposites of NiO/CuO based MOF rGO: an efficient and robust electrocatalyst for methanol oxidation in DMFC. Nanomaterials 10:1601
23. Yaqoob L, Noor T, Iqbal N, Nasir H, Zaman N (2019) Development of nickel-BTC-MOF-derived nanocomposite with rGO towards electrocatalytic oxidation of methanol and its product analysis. Catalysis 9:856
24. Yaqoob L, Noor T, Iqabal N, Nasir H, Sohail M, Zaman N, Usma M (2020) Nanocomposite of cobalt benzene tricarboxylic acid

MOF with rGO: an efficient and robust electrocatalyst for oxygen evolution reaction (OER). Renew Energy 156:1040–1054
25. Wahab A, Iqbal N, Noor T, Ashraf S, Raza MA, Ahmad A, Khan UA (2020) Thermally reduced mesoporous manganese MOF@reduced graphene oxide nanocomposite as bifunctional electrocatalyst for oxygen reduction and evolution. RSC Adv 10: 27728–27742
26. Haider MD, Iqbal N, Rizvi SAM, Noor T, Hanif S, Anwar R (2021) ZIF-67 derived Cu-doped electrocatalyst for oxygen reduction reaction. J Electrochem Energy Conv Stor 18:21001
27. Sarwar E, Noor T, Iqbal N, Mehmood Y, Ahmed S, Mehek R (2018) Effect of Co-Ni ratio in graphene based electro-catalyst for methanol oxidation. Fuel Cells 18:189–194
28. Hanif S, Shi X, Iqbal N, Noor T, Anwar R, Kannan AM (2019) ZIFderived PtNiCo/NC cathode catalyst for proton exchange membrane fuel cell. Appl Catal B Environ 258:117947
29. Noor T, Ammad M, Zaman N, Iqbal N, Yaqoob L, Nasir H (2019) A highly efficient and stable copper BTC metal organic framework derived electrocatalyst for oxidation of methanol in DMFC application. Catal Lett 149:3312–3327
30. Hanif S, Iqbal N, Shi X, Noor T, Ali G, Kannan AM (2020) NiCo-N-doped carbon nanotubes based cathode catalyst for alkaline membrane fuel cell. Renew Energy 154:508–516
31. Horiuchi Y, Toyao T, Saito M, Mochizuki K, Iwata M, Higashimura H, Anpo M, Matsuoka M (2012) Visible light promoted photocatalytic hydrogen production by using an amino-functionalized Ti (IV) metal-organic framework. J Phys Chem C 116:20848–20853
32. Fang S, Lichen B, Aliki M, Seunghwa L, Chao H, Laurent L, Xile H (2018) Transition metal oxides as electrocatalysts for the oxygen evolution reaction in alkaline solutions: an application-inspired renaissance. J Am Chem Soc 140:7748–7759
33. Yao Y, Yang Z, Sun H, Wang S (2012) Hydrothermal synthesis of Co_3O_4-graphene for heterogeneous activation of peroxymonosulfate for decomposition of phenol. Ind Eng Chem Res 51:14958–14965
34. Rahdar A, Aliahmad M, Azizi Y (2015) NiO nanoparticles: synthesis and characterization. J Nanostruct 5:145–151
35. Phiwadang K, Suphankij S, Mekprasart W, Pecharapa W (2013) Synthesis of CuO nanoparticles by precipitation method using different precursors. Energy Procedia 34:740–745
36. Adam RE, Pozina G, Willander M, Nur O (2018) Synthesis of ZnO nanoparticles by co-precipitation method for solar driven photodegradation of Congo red dye at different pH. Photonics Nanostruct Fundam Appl 32:11–18
37. Bordiga S, Lamberti C, Ricchiardi G, Regli L, Bonino F, Damin A, Lillerud KP, Bjorgen M, Zecchina A (2004) Electronic and vibrational properties of a MOF-5 metal-organic framework: ZnO quantum dot behavior. ChemCommun 20:2300–2301
38. Hu YH, Zhang L (2010) Amorphization of metal organic framework MOF-5 at unusually low applied pressure. Phys Rev B 81: 174103–174107
39. Hongyan X, Zhenyin H, Jiangtao D, Qiang Z, Libo G, Danfeng C, Junbin Z, Jun L, Chenyang X (2015) Synthesis and microwave absorption propertied of core shell structured Co_3O_4-PANI nanocomposite. J Nanomater 2015. https://doi.org/10.1155/2015/845983
40. Vinod V, Thekkae P, Miroslav C (2013) Green synthesis of copper oxide nanoparticles using gum karaya as a biotemplate and their antibacterial application. Int J Nanomedicine 8:889–898
41. Kalpana H, Sanjay B, Amit H, Prakash C, Kakasaheb M, Jalinder A, Nishigandh P, Vasant C (2014) Novel green route of synthesis of ZnO nanoparticles by using natural biodegradable polymer and its application as a catalyst for oxidation of aldehydes. J Macromol Sci A Pure Appl Chem 51:941–947